

Fixed Point Networks: Implicit Depth Models with Jacobian-Free Backprop

Samy Wu Fung*, Howard Heaton*, Qiuwei Li, Daniel McKenzie, Stanley Osher, Wotao Yin
Department of Mathematics
University of California Los Angeles

Abstract

A growing trend in deep learning replaces fixed depth models by approximations of the limit as network depth approaches infinity. This approach uses a portion of network weights to prescribe behavior by defining a limit condition. This makes network depth *implicit*, varying based on the provided data and an error tolerance. Moreover, existing implicit models can be implemented and trained with *fixed* memory costs in exchange for additional computational costs. In particular, backpropagation through implicit depth models requires solving a Jacobian-based equation arising from the implicit function theorem. We propose fixed point networks (FPNs), a simple setup for implicit depth learning that guarantees convergence of forward propagation to a unique limit defined by network weights and input data. Our key contribution is to provide a new Jacobian-free backpropagation (JFB) scheme that circumvents the need to solve Jacobian-based equations while maintaining fixed memory costs. This makes FPNs much cheaper to train and easy to implement. Our numerical examples yield state of the art classification results for implicit depth models and outperform corresponding explicit models.²

1 Introduction

A growing paradigm shift has emerged from explicit to implicit neural networks [2, 3, 6, 11, 21, 25, 32, 40, 45, 58, 67, 68]. In the entirely explicit setting, a neural network prescribes a series of computations that map input data d to an inference y . Networks can also explicitly leverage the assumption that high dimensional signals typically admit low dimensional representations in some latent space [12, 54, 57, 63, 64]. This may be done by designing the network to first map data to a latent space via a mapping Q_Θ and then apply a second mapping S_Θ to map the latent variable to the inference. Thus, an explicit network \mathcal{E}_Θ may take the compositional form

$$\mathcal{E}_\Theta(d) = S_\Theta(Q_\Theta(d)), \quad (1)$$

which is illustrated by the red arrows in Figure 1.

The mapping S_Θ may perform a number of computations to manipulate the latent variable u before mapping it to the inference. Inspired by this, implicit networks arose from the subsequent inquiry:

How can we model the limit as the latent space portion of network depth approaches infinity?

*Equal contribution

²Codes are available on Github: github.com/howardheaton/fixed_point_networks

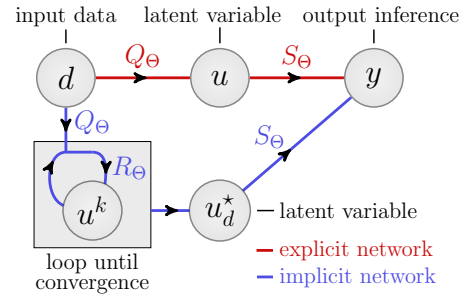


Figure 1: Explicit networks act by computing $S_\Theta \circ Q_\Theta$. Implicit networks add an equilibrium condition using R_Θ , which is applied repeatedly to update a latent variable u^k that estimates $u^* = R_\Theta(u^*; Q_\Theta(d))$.

The limit of latent space computations may be equivalently viewed as imposing some form of constraint on the latent space portion of the network. The repeated computations iteratively refine the current latent space variable until this condition, dependent on the input data d and the weights Θ , is satisfied. To formulate this limit condition, we introduce a third mapping R_Θ . Given data d , $R_\Theta(\cdot; Q(d))$ forms an operator on the latent space. The latent space condition is expressed using a fixed point equation, *i.e.*, we define an implicit fixed point network (FPN) \mathcal{M}_Θ by

$$\mathcal{M}_\Theta(d) \triangleq S_\Theta(u^*) \quad \text{where} \quad u^* = R_\Theta(u^*, Q_\Theta(d)). \quad (2)$$

Although the definition in (2) may be well-posed (with appropriate assumptions), it does not provide any indication about *how* to evaluate the network \mathcal{M}_Θ . This matter is discussed in Section 2 below.

Why Implicit? Implicit networks, and in particular FPNs, generalize the transition from residual neural networks (ResNets) [28] to continuous depth models [2, 6, 27, 67]. Implicit networks do not need to store intermediate quantities of the forward pass of a deep neural network for backpropagation. Instead, implicit models solve a Jacobian-based equation [2, 32, 67] or adjoint equation [6] arising from the implicit function theorem. Consequently, implicit models enable model training at *constant memory cost* – relieving a major bottleneck of training deep models. Moreover, infinite/implicit depth models are at least as expressible as explicit models [16, 21, 32]. This can also be observed by setting R_Θ in (2) to simply return Q_Θ ; in this case, the implicit network \mathcal{M}_Θ reduces to the explicit network \mathcal{E}_Θ in (1). Similar arguments are presented in [2, Theorem 3] to argue for the expressiveness of implicit depth networks. Universal approximation properties of implicit models then follow immediately from such properties of conventional deep neural networks (*e.g.* see [10, 34, 48]).

Contribution We first present a new class of neural networks, FPNs, that may be applied to several types of machine learning problems. FPNs are based on a fixed point problem formulation that ensures its forward propagation converges to a unique limit. Our primary contribution is to propose a new and simple Jacobian-free backpropagation (JFB) technique for training implicit depth networks that avoids solving the Jacobian-based equation arising from the implicit function theorem [37]. Instead, our scheme backpropagates by omitting the Jacobian term, resulting in a form of preconditioned gradient. This allows us to maintain the low-memory advantage of implicit depth models *and* avoid the extra computational costs that come with solving the Jacobian-based equation.

2 Fixed Point Network Formulation

Herein we formally cover our implicit depth formulation. All terms presented in this section are provided in a general context, which is made concrete in subsequent sections for each application. We include a subscript Θ on various terms to emphasize the indicated mapping will ultimately be parameterized in terms of tunable weights³ Θ . At the highest level, we are interested in constructing a neural network $\mathcal{M}_\Theta : \mathcal{D} \rightarrow \mathcal{Y}$ that maps from a data space⁴ \mathcal{D} and into an inference space \mathcal{Y} . The implicit portion of the computations occur in a latent space \mathcal{U} . We define a mapping $T_\Theta : \mathcal{U} \times \mathcal{D} \rightarrow \mathcal{U}$ and refer to this as the *network operator*, noting that fixing the input data yields an operator $T_\Theta(\cdot; d)$ on the latent space \mathcal{U} . Provided input data d , our aim is to find the unique fixed point u_d^* of $T_\Theta(\cdot; d)$ and then map u_d^* to the inference space \mathcal{Y} via a mapping $S_\Theta : \mathcal{U} \rightarrow \mathcal{Y}$. That is, we define

$$\mathcal{M}_\Theta(d) \triangleq S_\Theta(u_d^*) \quad \text{where} \quad u_d^* = T_\Theta(u_d^*, d). \quad (3)$$

For simplicity and computational efficiency, we assume T_Θ is defined as a composition so that it relates to the mapping $R_\Theta : \mathcal{U} \times \mathcal{U} \rightarrow \mathcal{U}$ in (2) by

$$T_\Theta(u; d) \triangleq R_\Theta(u, Q_\Theta(d)). \quad (4)$$

Implementation considerations for (4) are discussed below. Below we also introduce assumptions on T_Θ that

Algorithm 1 Fixed Point Network (Abstract Form)

1: $\mathcal{M}_\Theta(d) :$	\triangleleft Input data is d
2: $u^1 \leftarrow \tilde{u}$	\triangleleft Initialize inference
3: while $\ u - T_\Theta(u; d)\ > \varepsilon$	\triangleleft Loop to fixed point
4: $u^{k+1} \leftarrow T_\Theta(u^k; d)$	\triangleleft Refine latent variable
5: $k \leftarrow k + 1$	\triangleleft Increment counter
6: return $S_\Theta(u^k)$	\triangleleft Output inference

³We use the same subscript for all terms, noting each operator typically depends on a portion of the weights.

⁴Each space in this work is assumed to be a real-valued finite dimensional Hilbert space (*e.g.* \mathbb{R}^n) endowed with a product $\langle \cdot, \cdot \rangle$ and norm $\|\cdot\|$. It will be clear from context which space is being used.

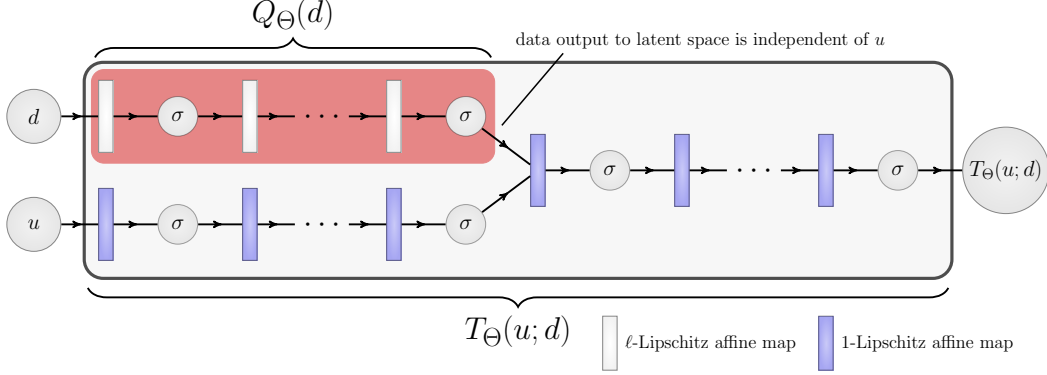


Figure 2: Diagram of a possible architecture for network operator T_Θ (in large rectangle). Data d and latent u variables are processed in two streams by nonlinearities (denoted by σ) and affine mappings (denoted by rectangles). These streams merge into a final stream that may also contain transformations. Light gray and blue affine maps are ℓ -Lipschitz and 1-Lipschitz, respectively. The mapping Q_Θ from data space to latent space is enclosed by the red rectangle.

yield sufficient conditions to use the simple procedure in Algorithm 1 to approximate $\mathcal{M}_\Theta(d)$. In this algorithm, the latent variable initialization \tilde{u} can be anything (e.g. the zero vector) since convergence is established independently of this choice. The inequality in Step 3 gives a fixed point residual condition that measures convergence. Step 4 implements a fixed point update. The estimate of the inference $\mathcal{M}_\Theta(d)$ is computed by applying S_Θ to the latent variable u in Step 5. In summary, Algorithm 1 describes the implicit network (blue path) in Figure 1.

Interpretation Multiple views of FPNs yield useful intuitions. Figure 1 provides the core diagram to keep in mind. The network repeatedly performs an operation, iteratively refining its “understanding” before outputting the final inference. For example, in image classification image data (encoded as d) are transformed into a latent space variable (encoded as u) in a “thought space” or “feature space.” The repeated application of T_Θ effectively acts as looking over parts of the image again and again until everything “sinks in.” The inference space is the translation of thoughts/features into classifications. Similarly, when analyzing sentiment of a sentence in natural language processing, FPNs read a sentence repeatedly until its understanding of the sentiment “makes sense.” Upon the final reading through the sentence, the network’s impression of the sentiment (in thought space) is consistent. Many instances require a single reading while more complex sentences may require rereads (e.g. see [2] for natural language processing experiments related to this).

A more classic viewpoint is to think of each fixed point as a solution to an optimization problem that models the learning task (as is typical in inverse problems). Network weights Θ are tuned to make the optimizer closely resemble the solution to the learning task. In this case, the network operator T_Θ behaves as an algorithmic update for iteratively solving the optimization problem (see Algorithm 1).

Convergence The guarantee of finitely many loops in Steps 3 and 4 of Algorithm 1 is a direct consequence of a classic functional analysis result by Banach [4]. This same approach is used by several implicit models [21, 32, 67]. A variation of this theorem for our setting is presented below.

Assumption 2.1. The mapping T_Θ is L -Lipschitz with respect to its inputs (u, d) , i.e. ,

$$\|T_\Theta(u_1; d_1) - T_\Theta(u_2; d_2)\| \leq L\|(u_1, d_1) - (u_2, d_2)\|, \text{ for all } (u_1, d_1), (u_2, d_2) \in \mathcal{U} \times \mathcal{D}. \quad (5)$$

Holding d fixed, the operator $T_\Theta(\cdot; d)$ is a contraction, i.e. there exists $\gamma \in [0, 1)$ such that

$$\|T_\Theta(u_1; d) - T_\Theta(u_2; d)\| \leq \gamma\|u_1 - u_2\|, \text{ for all } u_1, u_2 \in \mathcal{U}. \quad (6)$$

Remark 2.1. The L -Lipschitz condition on T_Θ is used since recent works show Lipschitz continuity with respect to inputs improves generalization [14, 24, 62] and adversarial robustness [1, 7].

Theorem 2.1. (BANACH) For any $u^1 \in \mathcal{U}$, if the sequence $\{u^k\}$ is generated via the update relation

$$u^{k+1} = T_\Theta(u^k; d), \text{ for all } k \in \mathbb{N}, \quad (7)$$

and if Assumption 2.1 holds, then $\{u^k\}$ converges to the unique fixed point u_d^* with R -linear rate.

Explicit \rightarrow Implicit As stated in the introduction, an implicit network is at least as expressive as an explicit network. The most straightforward way to transform an explicit network into an implicit network is to convert the hidden portion of the network into a fixed point operator. Given any explicit network (e.g. ResNet56 [28]), we may transform it into an implicit network in three steps. First, extract the hidden portion of the network and denote it by T_Θ . Next, make T_Θ a γ -contraction in u so that Assumption 2.1 holds (e.g. by replacing residual updates with convex combinations and by bounding singular values of each linear mapping). Lastly, denote the input layer which maps to the latent space by Q_Θ , and the final layer (e.g. the classification layer) by S_Θ . Completing these steps, our explicit network has transformed into the implicit FPN \mathcal{M}_Θ in Equation (2).

More intricate ways to go from explicit to implicit involve making the hidden portion of the given explicit network into *multiple* fixed point conditions. For instance, if a network transforms the features across different resolutions, we may set a fixed point condition at every resolution [3].

3 Backpropagation

We present a new and simple way to backpropagate with FPNs, called Jacobian-free backprop (JFB). Traditional backpropagation will *not* work effectively for FPNs since forward propagation during training could entail hundreds or thousands of iterations, requiring ever growing memory to store computational graphs. On the other hand, implicit methods maintain fixed memory costs by backpropagating “through the fixed point” and solving a Jacobian-based equation (at potentially substantial added computational costs). The key step to circumvent this Jacobian-based equation in our proposed method is to tune weights by using a preconditioned gradient. Let $\ell : \mathcal{Y} \times \mathcal{Y} \rightarrow \mathbb{R}$ be a smooth loss function, denoted by $\ell(x, y)$, and consider the problem

$$\min_{\Theta} \mathbb{E}_{d \sim \mathcal{D}} [\ell(y_d, \mathcal{M}_\Theta(d))], \quad (8)$$

where we abusively write \mathcal{D} to also mean a distribution. For clarity of presentation, in the remainder of this section we notationally suppress the dependencies on weights Θ by letting u_d^* denote the fixed point in (3). Unless noted otherwise, mapping arguments are implicit in this section; in each implicit case, this will correspond to the entries in (3). We begin with two standard assumptions that allow us to differentiate the network \mathcal{M}_Θ .

Assumption 3.1. *The mappings S_Θ and T_Θ are continuously differentiable with respect to u and Θ .*

Assumption 3.2. *The weights Θ may be written as a tuple $\Theta = (\theta_S, \theta_T)$ such that weight parameterization of S_Θ and T_Θ depend only on θ_S and θ_T , respectively.⁵*

Let \mathcal{J}_Θ be defined as the identity operator, denoted by I , minus the Jacobian⁶ of T_Θ at (u, d) , i.e.

$$\mathcal{J}_\Theta(u; d) \triangleq I - \frac{dT_\Theta}{du}(u; d). \quad (9)$$

Following backpropagation approaches for existing equilibrium models [2, 67], we can differentiate both sides of the fixed point relation in (3) to obtain, by the implicit function theorem,

$$\frac{du_d^*}{d\Theta} = \frac{\partial T_\Theta}{\partial u} \frac{du_d^*}{d\Theta} + \frac{\partial T_\Theta}{\partial \Theta} \implies \frac{du_d^*}{d\Theta} = \mathcal{J}_\Theta^{-1} \cdot \frac{\partial T_\Theta}{\partial \Theta}, \quad (10)$$

where \mathcal{J}_Θ^{-1} exists whenever \mathcal{J}_Θ exists (see Lemma A.1). Using the chain rule gives the loss gradient

$$\frac{d}{d\Theta} [\ell(y_d, \mathcal{M}_\Theta(d))] = \frac{\partial \ell}{\partial y} \left[\frac{dS_\Theta}{du} \frac{du^*}{d\Theta} + \frac{\partial S_\Theta}{\partial \Theta} \right] = \frac{\partial \ell}{\partial y} \left[\frac{dS_\Theta}{du} \mathcal{J}_\Theta^{-1} \frac{\partial T_\Theta}{\partial \Theta} + \frac{\partial S_\Theta}{\partial \Theta} \right]. \quad (11)$$

The matrix \mathcal{J}_Θ satisfies the coercivity inequality (see Lemma A.1)

$$\langle u, \mathcal{J}_\Theta^{-1} u \rangle \geq \frac{1 - \gamma}{(1 + \gamma)^2} \|u\|^2, \quad \text{for all } u \in \mathcal{U}. \quad (12)$$

Intuitively, this property makes it seem possible to remove \mathcal{J}_Θ^{-1} from (11) and backpropagate using

$$p_\Theta \triangleq - \frac{\partial \ell}{\partial y} \left(\frac{dS_\Theta}{du} \frac{\partial T_\Theta}{\partial \Theta} + \frac{\partial S_\Theta}{\partial \Theta} \right). \quad (13)$$

⁵This assumption is easy to ensure in practice. For notational brevity, we use the subscript Θ throughout.

⁶Under Assumption 2.1, the Jacobian \mathcal{J}_Θ exists almost everywhere. However, the presentation is much cleaner by assuming smoothness.

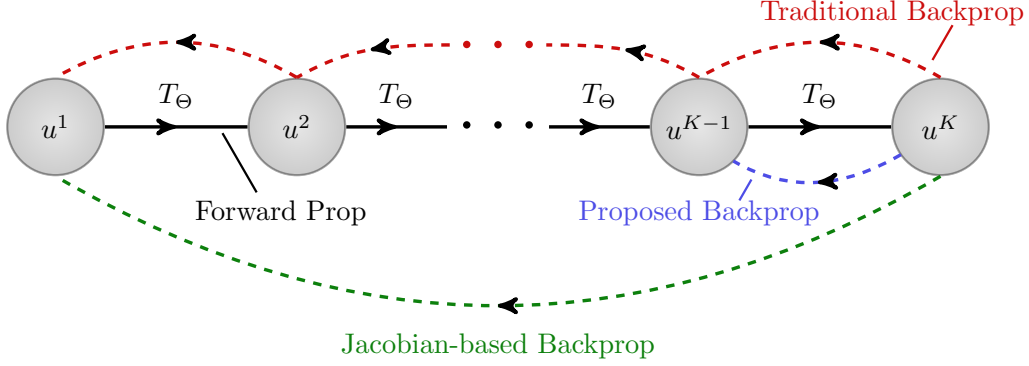


Figure 3: Diagram of backpropagation schemes for recurrent implicit depth and fixed depth models. Forward propagation is tracked via solid arrows point to the right. Backpropagation is shown via dashed arrows pointing to the left. For sake of illustration, in this diagram we assume the depth of feed forward propagation happens to agree between the traditional fixed depth feed forward approach and the implicit depth approaches; however, this is not true in general.

The omission of \mathcal{J}_Θ^{-1} admits to two straightforward interpretations. First note p_Θ is precisely the gradient of the expression $\ell(y_d, S_\Theta(T_\Theta(u_d^*; d)))$, treating u_d^* as a constant *independent* of Θ . Furthermore, the argument $S_\Theta(T_\Theta(u_d^*; d))$ yields the *same* output as $\mathcal{M}_\Theta(d)$. The distinction is that using $S_\Theta(T_\Theta(u_d^*; d))$ assumes, perhaps by chance, the user chose the first iterate u^1 in their fixed point iteration (see Algorithm 1) to be precisely the fixed point u_d^* . This makes the iteration trivial, “converging” in one iteration. We can simulate this behavior by using the fixed point iteration to find u_d^* and only backpropagating through the final step of the fixed point iteration, as shown in Figure 3.

The second interpretation of our approach is to view our backpropagation as a form of preconditioned gradient descent. Since the weights Θ typically lay in a space of much higher dimension than the latent space \mathcal{U} , the Jacobians $\partial S_\Theta / \partial \Theta$ and $\partial T_\Theta / \partial \Theta$ will effectively always have full column rank. We leverage this fact via the following assumption.

Assumption 3.3. Under Assumption 3.2, given any weights $\Theta = (\theta_S, \theta_T)$ and data d , the matrix

$$M \triangleq \begin{bmatrix} \frac{\partial S_\Theta}{\partial \theta_S} & 0 \\ 0 & \frac{\partial T_\Theta}{\partial \theta_T} \end{bmatrix} \quad (14)$$

has full column rank and is sufficiently well conditioned to satisfy the inequality⁷

$$\kappa(M^\top M) = \frac{\lambda_{\max}(M^\top M)}{\lambda_{\min}(M^\top M)} \leq \frac{1}{\gamma}. \quad (15)$$

Remark 3.1. The conditioning portion of the above assumption is useful for bounding the worst-case behavior in our analysis. However, we found it unnecessary to enforce this in our experiments for effective training (e.g. see Figure 5), which we hypothesize is justified because worst case behavior rarely occurs in practice and we train using averages of p_Θ for samples drawn from a large data set.

The full column rank of M enables us to rewrite p_Θ as a preconditioned gradient, i.e.

$$p_\Theta = \underbrace{\left(M \begin{bmatrix} \mathbf{I} & 0 \\ 0 & \mathcal{J}_\Theta \end{bmatrix} M^+ \right)}_{\text{preconditioning term}} \frac{d\ell}{d\Theta}, \quad (16)$$

where M^+ is the Moore-Penrose pseudo inverse [49, 56]. These insights lead to our main result.

Theorem 3.1. If Assumptions 2.1, 3.1, 3.2, and 3.3 hold for given weights Θ and data d , then

$$p_\Theta \triangleq - \left[\frac{\partial \ell}{\partial y} \left(\frac{dS_\Theta}{du} \frac{\partial T_\Theta}{\partial \Theta} + \frac{\partial S_\Theta}{\partial \Theta} \right) \right]_{(u,d)=(u_d^*,d)} \quad (17)$$

forms a descent direction for $\ell(y_d, \mathcal{M}_\Theta(d))$ with respect to Θ .

⁷The term γ here refers to the contraction factor in (6).

Theorem 3.1 has two practical implications. The first is we can leverage the memory efficiency of implicit depth models where memory cost is constant with respect to the “depth”, *i.e.* number of applications of T_Θ . The second takeaway is we can avoid difficult computations associated with \mathcal{J}_Θ^{-1} in (11) (*i.e.* solving an associated linear system/adjoint equation) in implicit depth literature [2, 6, 11, 67]. Thus, our scheme more naturally applies to general multilayered T_Θ and is substantially simpler to code. Our scheme is juxtaposed in Figure 3 with classic and Jacobian-based schemes.

Two additional considerations must be made when determining the efficacy of training a network using (17) rather than Jacobian-based gradients (11):

- Does use of (17) degrade training/testing performance relative to (11)?
- Is the gradient (17) resilient to errors in estimates of the fixed point u_d^* ?

The first answer is that our training scheme simply takes a different path to minimizers than using gradients with the implicit model. Thus, for nonconvex problems, one should not expect the results to be the same. Our experiments (see Section 5) using (17) for training yield state-of-the-art results. Furthermore, (17) outperforms (11) in our experiments (when applied to identical models). This leads us to believe, on experimental grounds, that (17) is at least as effective as (11). The second inquiry is answered in part by the following corollary, which states our proposed approach yields descent even when an approximation of the fixed point u_d^* is used.

Corollary 3.1. *Given weights Θ and data d , there exists $\varepsilon > 0$ such that if $u_d^\varepsilon \in \mathcal{U}$ satisfies $\|u_d^\varepsilon - u_d^*\| \leq \varepsilon$ and the assumptions of Theorem 3.1 hold, then*

$$p_\Theta^\varepsilon \triangleq - \left[\frac{\partial \ell}{\partial y} \left(\frac{dS_\Theta}{du} \frac{\partial T_\Theta}{\partial \Theta} + \frac{\partial S_\Theta}{\partial \Theta} \right) \right]_{(u,d)=(u_d^\varepsilon,d)} \quad (18)$$

is a descent direction for the loss function $\ell(y_d, \mathcal{M}_\Theta(u_d^, d))$ with respect to Θ .*

We are not aware of any analogous results for error tolerances in the implicit depth literature.

Coding Backpropagation The backpropagation of our scheme is very similar to that of a standard backpropagation. We illustrate this in the sample of PyTorch [55] code in Figure 4. Here `explicit_model` represents $S_\Theta(T_\Theta(u; d))$. The fixed point `u_fxd_pt` is computed by successively applying T_Θ (see Algorithm 1) in `eval` mode. With this fixed point, `explicit_model` evaluates and returns $S_\Theta(T_\Theta(u_d^*, d))$ to `y`

Implicit Forward + Proposed Backprop

```
u_fxd_pt = find_fixed_point(in_feature)
y = explicit_model(u_fxd_pt, in_feature)
loss = criterion(y, labels)
loss.backward()
optimizer.step()
```

Figure 4: Sample PyTorch code for backpropagation⁸

in `train` mode (to create the computational graph). Thus, our scheme coincides with standard backpropagation through an explicit network with *one* latent space layer. On the other hand, standard implicit models backpropagate by solving a linear system to apply \mathcal{J}_Θ^{-1} as in (11). That approach also requires users to manually update the parameters, use more computational resources, and make considerations (*e.g.* conditioning of \mathcal{J}_Θ^{-1}) for the particular network architecture used.

4 Related Works

Continuous Network Models A well-known example of models based on a continuous view of deep networks is neural ODEs [6, 11, 60]. Neural ODEs leverage known connections between deep residual networks and discretizations of differential equations [5, 15, 27, 47, 59, 66], and replace these discretizations by black-box ODE solvers in forward and backward passes. The implicit property of these models arise from their method for computing gradients. Rather than backpropagate through each layer, backpropagation is instead done by solving the adjoint equation [31] using a blackbox ODE solver as well. This allows the user to alleviate the memory costs of backpropagation through deep neural networks by solving the adjoint equation at additional computational costs. A drawback is that the adjoint equation must be solved to high-accuracy; otherwise, a descent direction is not necessarily guaranteed [22, 52, 53, 69]. Another related work [23] uses reversible residual

⁸Please see our implemented codes for complete details.

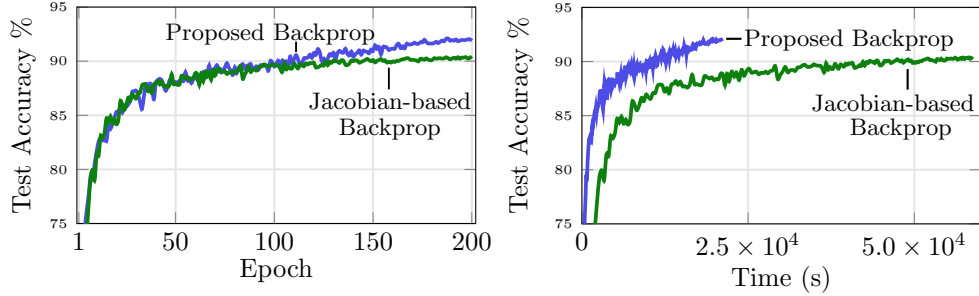


Figure 5: CIFAR10 performance using identical models/configurations, but with two backpropagation schemes: our proposed method (blue) and the standard Jacobian-based backpropagation in (11) (green), with fixed point tolerance $\epsilon = 10^{-4}$. Our method is faster and yields better test accuracy.

networks (ResNets) to achieve fixed memory costs; this is similar in spirit to the present work, but it is specialized to ResNets and, as the authors noted, is prone to accumulating numerical errors since it backpropagates through all layers (unlike FPNs). We further note the adjoint equation for these models is analogous to the linear system that is solved in fixed point models (discussed next).

Fixed Point Models Another class of implicit models involve formulating machine learning tasks as fixed point problems. Deep Equilibrium (DEQ) Networks [2] find a fixed point of a non-linear dynamical system corresponding to an effectively infinite-depth “weight-tied, input-injected” network. In this setting, forward propagation consists of applying a root-finding method to find a fixed point, and backpropagation involves solving a Jacobian-based equation arising from the implicit function theorem [37]. Multiscale DEQs (MD-EQs) [3] expands upon DEQs by learning multiple feature resolutions simultaneously. As is well known in fixed point theory, naïve forward propagation of a fixed point scheme is not necessarily stable. To this end, Monotone Operator Equilibrium Networks (MON) [67] leverage monotone operator theory to create stable forward and backward propagation by using special network architectures. These networks must be 1-layer networks with activations based on proximal operators (e.g. ReLU). Similarly to MON, FPNs leverage fixed point theory. However, our approach generalizes MONs by allowing a wider class of network architectures. And, while our approach falls under the category of implicit depth models, our backpropagation scheme *circumvents* the need to solve the Jacobian-based equation presented in (9). In [21] the need to solve a Jacobian-based equation is also avoided by eschewing backprop entirely and using the so-called

MNIST

Method	Model size	Acc.
Explicit (Fully Connected)	84K	98.2%
MON (Fully Connected) [‡]	84K	98.2%
FPN (Fully Connected)	84K	98.6%

Explicit (Convolution)	84K	99.4%
Neural ODE [†] (Convolution)	84K	96.4%
Aug. Neural ODE [†] (Convolution)	84K	98.2%
MON (Convolution) [‡]	84K	99.2%
FPN (Convolution)	84K	99.5%

SVHN

Method	Model size	Acc.
Explicit	154K	92.4%
Neural ODE [†]	172K	81.0%
Aug. Neural ODE [†]	172K	83.5%
MON (Single conv) [‡]	172K	88.8%
MON (Multi-tier lg) [‡]	170K	92.3%
FPN (ours)	154K	92.8%

CIFAR-10

Method	Model size	Acc.
Explicit	172K	80.1%
Neural ODE [†]	172K	53.7%
Aug. Neural ODE [†]	172K	60.6%
MON (Single conv) [‡]	172K	74.1%
FPN (ours)	172K	80.7%

MON (Multi-tier lg) ^{‡*}	1.01M	89.7%
FPN (ours)*	860K	92.1%

Table 1: Test accuracy of FPNs (our method) compared to Neural ODEs, Augmented Neural ODEs, and MONs; [†]as reported in [11]; [‡]as reported in [67]; *with data augmentation

	Dataset	Avg time per epoch (s)	# of \mathcal{J} mat-vec products	Accuracy %
With Jacobian (Standard)	MNIST	218.5	5.9×10^8	99.0
	SVHN	186.3	2.3×10^8	90.6
	CIFAR10	293.8	4.4×10^8	90.5
Jacobian-free (Proposed)	MNIST	50.2	0	99.5
	SVHN	56.7	0	92.7
	CIFAR10	105.4	0	92.1

Table 2: Backpropagation comparison for FPN using the Jacobian-based equation (first three rows) and our proposed Jacobian-free backpropagation. “Mat-vecs” denotes matrix-vector products.

“Fenchel divergence formulation” of the training loss. However, that approach appears to be computationally taxing, and the authors do not implement it on any large-scale benchmark data sets.

5 Experiments

We demonstrate the effectiveness of our backpropagation scheme on FPNs. Experiments are done using PyTorch [55]. All networks were designed such that Assumptions 2.1 and 3.2 hold.⁹ In particular, we bound the largest singular values of latent space network mappings and choose standard 1-Lipschitz activations functions (*e.g.* see [8, 9, 20]). All experiments are run on a single NVIDIA TITAN X GPU with 12GB RAM. More details about experimental settings can be found in Appendix B.

5.1 Classification

We train FPNs on three benchmark image classification datasets: SVHN [51], MNIST [41], and CIFAR-10 [39]. Table 1 compares our results with state-of-the-art results for implicit models, including Neural ODEs [6], Augmented Neural ODEs [11], and MONs [67]. We also compare with an explicit version of our FPNs given in (1). The explicit models are trained with the exact same setup as those used for FPN (with the exception of using one latent space layer). Table 1 shows FPNs, trained with our scheme, substantially outperform all the ODE-based models as well as MONs using similar or fewer parameters. Appendix C contains further experimental details.

5.2 Comparing Backpropagation

Table 2 compares the performance between using the standard Jacobian-based backpropagation and our proposed backpropagation. The experiments are performed on all the datasets described in Section 5.1. To apply the Jacobian-based in (10), we use the conjugate gradient (CG) method on an associated set of normal equations in similar manner to [43]. We set a maximum of 500 CG iterations. The remainder of the experimental settings are kept the same as those from our proposed approach (and are therefore not tuned to the best of our ability). The main purpose of the Jacobian-based results in Figure 5 and Table 2, are the significant speedups in training time (in each case obtaining roughly 2X or more speedup) while maintaining a competitive accuracy that outperforms previous state-of-the-art implicit models. Further plots and comparisons are provided in Appendix B.

6 Conclusion

We present Fixed Point Networks (FPNs), a class of models that generalizes existing implicit models to a wider choice of architectures (while maintaining convergence guarantees). A new and simple Jacobian-free backpropagation (JFB) scheme is proposed that avoids solving a Jacobian-based equation. This enables our approach to enjoy fixed memory costs (regardless of depth), be easy to code, and yield faster backpropagation than previously possible. We show our scheme is theoretically justified (even with errors present). Our experiments also show our scheme is efficient and effective. Extensions to FPNs will enable satisfaction of additional constraints for imaging and phase retrieval [13, 19, 29, 33, 36], geophysics [17, 18, 26], and game theory [42, 44, 50, 61, 65].

⁹A weaker version of Assumption 3.1 also holds in practice, *i.e.* differentiability almost everywhere.

Broader Impact

The rapid rise of deep learning has been largely due to the growth in computational capabilities. Despite this, a key shortcoming associated with creating deep learning models is that making them deeper and, thus, more expressible requires ever increasing memory. Thus, for practical devices, computer memory limits model depth. Existing implicit depth networks present a way of circumventing this memory limit; however, this comes with the trade off of much more computational costs to train networks. This work presents a third option, implicit depth *without* increasing the computational costs of training. This approach increases the efficiency of computational resources both with respect to memory and computation. Moreover, by using implicit depth models, the same model can be deployed with settings attuned to both high power (*e.g.* servers) and low power (*e.g.* mobile) devices.

Acknowledgments and Disclosure of Funding

Samy Wu Fung and Stanley Osher are supported by AFOSR MURI FA9550-18-1-0502, AFOSR Grant No. FA9550-18-1-0167, and ONR Grants N00014-18-1-2527 and N00014-17-1-21. Daniel McKenzie and Qiuwei Li are supported by AFOSR MURI FA9550-18-1-0502. Howard Heaton is supported by the National Science Foundation (NSF) Graduate Research Fellowship under Grant No. DGE-1650604. Any opinion, findings, and conclusions or recommendations expressed in this material are those of the authors and do not necessarily reflect the views of the NSF.

References

- [1] C. Anil, J. Lucas, and R. Grosse. Sorting out lipschitz function approximation. In *International Conference on Machine Learning*, pages 291–301. PMLR, 2019.
- [2] S. Bai, J. Z. Kolter, and V. Koltun. Deep equilibrium models. In *Advances in Neural Information Processing Systems*, pages 690–701, 2019.
- [3] S. Bai, V. Koltun, and J. Z. Kolter. Multiscale deep equilibrium models. *Advances in Neural Information Processing Systems*, 33, 2020.
- [4] S. Banach. Sur les opérations dans les ensembles abstraits et leur application aux équations intégrales. *Fund. math*, 3(1):133–181, 1922.
- [5] B. Chang, L. Meng, E. Haber, L. Ruthotto, D. Begert, and E. Holtham. Reversible architectures for arbitrarily deep residual neural networks. In *Proceedings of the AAAI Conference on Artificial Intelligence*, volume 32, 2018.
- [6] R. T. Chen, Y. Rubanova, J. Bettencourt, and D. K. Duvenaud. Neural ordinary differential equations. In *Advances in neural information processing systems*, pages 6571–6583, 2018.
- [7] M. Cisse, P. Bojanowski, E. Grave, Y. Dauphin, and N. Usunier. Parseval networks: Improving robustness to adversarial examples. In *International Conference on Machine Learning*, pages 854–863. PMLR, 2017.
- [8] P. L. Combettes and J.-C. Pesquet. Deep neural network structures solving variational inequalities. *Set-Valued and Variational Analysis*, pages 1–28, 2020.
- [9] P. L. Combettes and J.-C. Pesquet. Lipschitz certificates for layered network structures driven by averaged activation operators. *SIAM Journal on Mathematics of Data Science*, 2(2):529–557, 2020.
- [10] B. C. Csáji et al. Approximation with artificial neural networks. *Faculty of Sciences, Eötvös Loránd University, Hungary*, 24(48):7, 2001.
- [11] E. Dupont, A. Doucet, and Y. W. Teh. Augmented neural odes. In *Advances in Neural Information Processing Systems*, volume 32. Curran Associates, Inc., 2019.
- [12] M. Elad, M. A. Figueiredo, and Y. Ma. On the role of sparse and redundant representations in image processing. *Proceedings of the IEEE*, 98(6):972–982, 2010.

- [13] J. R. Fienup. Phase retrieval algorithms: a comparison. *Applied optics*, 21(15):2758–2769, 1982.
- [14] C. Finlay, J. Calder, B. Abbasi, and A. Oberman. Lipschitz regularized deep neural networks generalize and are adversarially robust. *arXiv preprint arXiv:1808.09540*, 2018.
- [15] C. Finlay, J.-H. Jacobsen, L. Nurbekyan, and A. M. Oberman. How to train your neural ode. *arXiv preprint arXiv:2002.02798*, 2020.
- [16] J. Frecon, S. Salzo, and M. Pontil. Bilevel learning of deep representations. 2021.
- [17] S. W. Fung and L. Ruthotto. A multiscale method for model order reduction in pde parameter estimation. *Journal of Computational and Applied Mathematics*, 350:19–34, 2019.
- [18] S. W. Fung and L. Ruthotto. An uncertainty-weighted asynchronous admm method for parallel pde parameter estimation. *SIAM Journal on Scientific Computing*, 41(5):S129–S148, 2019.
- [19] S. W. Fung and Z. Wendy. Multigrid optimization for large-scale ptychographic phase retrieval. *SIAM Journal on Imaging Sciences*, 13(1):214–233, 2020.
- [20] B. Gao and L. Pavel. On the properties of the softmax function with application in game theory and reinforcement learning. *arXiv preprint arXiv:1704.00805*, 2017.
- [21] L. E. Ghaoui, F. Gu, B. Travacca, A. Askari, and A. Y. Tsai. Implicit deep learning. *arXiv preprint arXiv:1908.06315*, 2019.
- [22] A. Gholami, K. Keutzer, and G. Biros. Anode: Unconditionally accurate memory-efficient gradients for neural odes. *arXiv preprint arXiv:1902.10298*, 2019.
- [23] A. N. Gomez, M. Ren, R. Urtasun, and R. B. Grosse. The reversible residual network: Back-propagation without storing activations. *arXiv preprint arXiv:1707.04585*, 2017.
- [24] H. Gouk, E. Frank, B. Pfahringer, and M. J. Cree. Regularisation of neural networks by enforcing Lipschitz continuity. *Machine Learning*, 110(2):393–416, Feb. 2021.
- [25] S. Gould, R. Hartley, and D. Campbell. Deep declarative networks: A new hope. *arXiv preprint arXiv:1909.04866*, 2019.
- [26] E. Haber. *Computational methods in geophysical electromagnetics*. SIAM, 2014.
- [27] E. Haber and L. Ruthotto. Stable architectures for deep neural networks. *Inverse Problems*, 34(1):014004, 2017.
- [28] K. He, X. Zhang, S. Ren, and J. Sun. Deep residual learning for image recognition. In *Proceedings of the IEEE conference on computer vision and pattern recognition*, pages 770–778, 2016.
- [29] H. Heaton, S. W. Fung, A. T. Lin, S. Osher, and W. Yin. Projecting to manifolds via unsupervised learning. *arXiv preprint arXiv:2008.02200*, 2020.
- [30] Y. Idelbayev. Proper ResNet implementation for CIFAR10/CIFAR100 in PyTorch. https://github.com/akamaster/pytorch_resnet_cifar10. Accessed: 2021-03-15.
- [31] A. Jameson. Aerodynamic design via control theory. *Journal of scientific computing*, 3(3):233–260, 1988.
- [32] Y. Jeon, M. Lee, and J. Y. Choi. Differentiable forward and backward fixed-point iteration layers. *IEEE Access*, 2021.
- [33] K. Kan, S. W. Fung, and L. Ruthotto. Pnkh-b: A projected newton-krylov method for large-scale bound-constrained optimization. *arXiv preprint arXiv:2005.13639*, 2020.
- [34] P. Kidger and T. Lyons. Universal approximation with deep narrow networks. In *Conference on Learning Theory*, pages 2306–2327. PMLR, 2020.
- [35] D. P. Kingma and J. Ba. Adam: A method for stochastic optimization. In *ICLR (Poster)*, 2015.

- [36] M. V. Klibanov. Determination of a compactly supported function from the argument of its fourier transform. In *Doklady Akademii Nauk*, volume 289, pages 539–540. Russian Academy of Sciences, 1986.
- [37] S. G. Krantz and H. R. Parks. *The implicit function theorem: history, theory, and applications*. Springer Science & Business Media, 2012.
- [38] E. Kreyszig. *Introductory Functional Analysis with Applications*, volume 1. Wiley New York, 1978.
- [39] A. Krizhevsky and G. Hinton. Learning multiple layers of features from tiny images. Technical report, University of Toronto, 2009.
- [40] N. Lawrence, P. Loewen, M. Forbes, J. Backstrom, and B. Gopaluni. Almost surely stable deep dynamics. In H. Larochelle, M. Ranzato, R. Hadsell, M. F. Balcan, and H. Lin, editors, *Advances in Neural Information Processing Systems*, volume 33, pages 18942–18953. Curran Associates, Inc., 2020.
- [41] Y. LeCun, C. Cortes, and C. Burges. Mnist handwritten digit database. *ATT Labs [Online]*. Available: <http://yann.lecun.com/exdb/mnist>, 2, 2010.
- [42] S. Li, Y. Xie, Q. Li, and G. Tang. Cubic regularization for differentiable games. In *NeurIPS Workshop 2019*.
- [43] R. Liao, Y. Xiong, E. Fetaya, L. Zhang, K. Yoon, X. Pitkow, R. Urtasun, and R. Zemel. Reviving and improving recurrent back-propagation. In *International Conference on Machine Learning*, pages 3082–3091. PMLR, 2018.
- [44] A. T. Lin, S. W. Fung, W. Li, L. Nurbekyan, and S. J. Osher. Apac-net: Alternating the population and agent control via two neural networks to solve high-dimensional stochastic mean field games. *arXiv preprint arXiv:2002.10113*, 2020.
- [45] A. Look, S. Doneva, M. Kandemir, R. Gemulla, and J. Peters. Differentiable implicit layers. *arXiv preprint arXiv:2010.07078*, 2020.
- [46] I. Loshchilov and F. Hutter. Sgdr: Stochastic gradient descent with warm restarts. *arXiv preprint arXiv:1608.03983*, 2016.
- [47] Y. Lu, A. Zhong, Q. Li, and B. Dong. Beyond finite layer neural networks: Bridging deep architectures and numerical differential equations. In *International Conference on Machine Learning*, pages 3276–3285. PMLR, 2018.
- [48] Z. Lu, H. Pu, F. Wang, Z. Hu, and L. Wang. The expressive power of neural networks: A view from the width. *arXiv preprint arXiv:1709.02540*, 2017.
- [49] E. H. Moore. On the reciprocal of the general algebraic matrix. *Bulletin of the American Mathematical Society*, 26:394–395, 1920.
- [50] R. B. Myerson. *Game theory*. Harvard university press, 2013.
- [51] Y. Netzer, T. Wang, A. Coates, A. Bissacco, B. Wu, and A. Y. Ng. Reading digits in natural images with unsupervised feature learning. In *NIPS Workshop on Deep Learning and Unsupervised Feature Learning*, 2011.
- [52] D. Onken, S. W. Fung, X. Li, and L. Ruthotto. OT-Flow: Fast and accurate continuous normalizing flows via optimal transport. *arXiv preprint arXiv:2006.00104*, 2020.
- [53] D. Onken and L. Ruthotto. Discretize-optimize vs. optimize-discretize for time-series regression and continuous normalizing flows. *arXiv preprint arXiv:2005.13420*, 2020.
- [54] S. Osher, Z. Shi, and W. Zhu. Low dimensional manifold model for image processing. *SIAM Journal on Imaging Sciences*, 10(4):1669–1690, 2017.
- [55] A. Paszke, S. Gross, S. Chintala, G. Chanan, E. Yang, Z. DeVito, Z. Lin, A. Desmaison, L. Antiga, and A. Lerer. Automatic differentiation in pytorch. 2017.

- [56] R. Penrose. A generalized inverse for matrices. In *Mathematical Proceedings of the Cambridge Philosophical Society*, volume 51, pages 406–413. Cambridge University Press, 1955.
- [57] G. Peyré. Manifold models for signals and images. *Computer vision and image understanding*, 113(2):249–260, 2009.
- [58] M. Revay and I. Manchester. Contracting implicit recurrent neural networks: Stable models with improved trainability. In *Learning for Dynamics and Control*, pages 393–403. PMLR, 2020.
- [59] L. Ruthotto and E. Haber. Deep neural networks motivated by partial differential equations. *Journal of Mathematical Imaging and Vision*, pages 1–13, 2019.
- [60] L. Ruthotto and E. Haber. An introduction to deep generative modeling. *arXiv preprint arXiv:2103.05180*, 2021.
- [61] L. Ruthotto, S. J. Osher, W. Li, L. Nurbekyan, and S. W. Fung. A machine learning framework for solving high-dimensional mean field game and mean field control problems. *Proceedings of the National Academy of Sciences*, 117(17):9183–9193, 2020.
- [62] J. Sokolić, R. Giryes, G. Sapiro, and M. R. Rodrigues. Robust large margin deep neural networks. *IEEE Transactions on Signal Processing*, 65(16):4265–4280, 2017.
- [63] M. Udell and A. Townsend. Why are big data matrices approximately low rank? *SIAM Journal on Mathematics of Data Science*, 1(1):144–160, 2019.
- [64] L. Van der Maaten and G. Hinton. Visualizing data using t-sne. *Journal of machine learning research*, 9(11), 2008.
- [65] J. Von Neumann. On the theory of games of strategy. *Contributions to the Theory of Games*, 4:13–42, 1959.
- [66] E. Weinan. A proposal on machine learning via dynamical systems. *Communications in Mathematics and Statistics*, 5(1):1–11, 2017.
- [67] E. Winston and J. Z. Kolter. Monotone operator equilibrium networks. In H. Larochelle, M. Ranzato, R. Hadsell, M. F. Balcan, and H. Lin, editors, *Advances in Neural Information Processing Systems*, volume 33, pages 10718–10728. Curran Associates, Inc., 2020.
- [68] Q. Zhang, Y. Gu, M. Mateusz, M. Baktashmotlagh, and A. Eriksson. Implicitly defined layers in neural networks. *arXiv preprint arXiv:2003.01822*, 2020.
- [69] T. Zhang, Z. Yao, A. Gholami, K. Keutzer, J. Gonzalez, G. Biros, and M. Mahoney. Anodev2: A coupled neural ode evolution framework. *arXiv preprint arXiv:1906.04596*, 2019.

A Proofs

This section provides proofs for the results of Section 3. For the reader's convenience, we restate all results before proving them.

Lemma A.1. *If Assumption 2.1 and 3.1 hold, then \mathcal{J}_Θ in (9) exists and*

$$\langle u, \mathcal{J}_\Theta u \rangle \geq (1 - \gamma) \|u\|^2, \quad \text{for all } u \in \mathcal{U}. \quad (19)$$

Additionally, \mathcal{J}_Θ is invertible, and its inverse \mathcal{J}_Θ^{-1} satisfies the coercivity inequality

$$\langle u, \mathcal{J}_\Theta^{-1} u \rangle \geq \frac{1 - \gamma}{(1 + \gamma)^2} \|u\|^2, \quad \text{for all } u \in \mathcal{U}. \quad (20)$$

Proof. We proceed in the following manner. First we establish the coercivity inequality (19) (Step 1). This is used to show \mathcal{J}_Θ is invertible (Step 2). The previous two results are then combined to establish the inequality (20) (Step 3). All unproven results that are quoted below about operators are standard and may be found in any standard functional analysis text (e.g. [38]).

Step 1. To obtain our coercivity inequality, we identify a bound on the operator norm for $\partial T_\Theta / \partial u$. Fix any unit vector $v \in \mathcal{U}$. Then, by the definition of differentiation,

$$\frac{dT_\Theta}{du} v = \lim_{\varepsilon \rightarrow 0^+} \frac{T_\Theta(u^* + \varepsilon v; d) - T_\Theta(u^*; d)}{\|(u^* + \varepsilon v) - u^*\|} = \lim_{\varepsilon \rightarrow 0^+} \frac{T_\Theta(u^* + \varepsilon v; d) - T_\Theta(u^*; d)}{\varepsilon}. \quad (21)$$

Thus,

$$\left\| \frac{dT_\Theta}{du} v \right\| = \left\| \lim_{\varepsilon \rightarrow 0^+} \frac{T_\Theta(u^* + \varepsilon v; d) - T_\Theta(u^*; d)}{\varepsilon} \right\| = \lim_{\varepsilon \rightarrow 0^+} \frac{\|T_\Theta(u^* + \varepsilon v; d) - T_\Theta(u^*; d)\|}{\varepsilon}, \quad (22)$$

where the first equality follows from (21) and the second holds by the continuity of norms. Combining (23) with the Lipschitz assumption (6) gives the upper bound

$$\left\| \frac{dT_\Theta}{du} v \right\| \leq \lim_{\varepsilon \rightarrow 0^+} \frac{\gamma \|(u^* + \varepsilon v) - u^*\|}{\varepsilon} = \gamma. \quad (23)$$

Because the upper bound relation in (23) holds for an arbitrary unit vector $v \in \mathcal{U}$, we deduce

$$\left\| \frac{dT_\Theta}{du} \right\| \triangleq \sup \left\{ \left\| \frac{dT_\Theta}{du} v \right\| : \|v\| = 1 \right\} \leq \gamma. \quad (24)$$

That is, the operator norm is bounded by γ . Together the Cauchy-Schwarz inequality and (24) imply

$$\left\langle u, \frac{dT_\Theta}{du} u \right\rangle \leq \left\| \frac{dT_\Theta}{du} \right\| \|u\|^2 \leq \gamma \|u\|^2, \quad \text{for all } u \in \mathcal{U}. \quad (25)$$

Whence the bilinear form $\langle \cdot, \mathcal{J}_\Theta \cdot \rangle$ is $(1 - \gamma)$ coercive, i.e.

$$\langle u, \mathcal{J}_\Theta u \rangle = \|u\|^2 - \left\langle u, \frac{dT_\Theta}{du} u \right\rangle \geq (1 - \gamma) \|u\|^2, \quad \text{for all } u \in \mathcal{U}. \quad (26)$$

Step 2. Consider any kernel element $w \in \ker(\mathcal{J}_\Theta)$. Then (26) implies

$$(1 - \gamma) \|w\|^2 \leq \langle w, \mathcal{J}_\Theta w \rangle = \langle w, 0 \rangle = 0 \implies (1 - \gamma) \|w\|^2 \leq 0 \implies w = 0. \quad (27)$$

Consequently, the kernel of \mathcal{J}_Θ is trivial, i.e.

$$\ker(\mathcal{J}_\Theta) \triangleq \{u : \mathcal{J}_\Theta u = 0\} = \{0\}. \quad (28)$$

Thus, the linear operator \mathcal{J}_Θ is invertible.

Step 3. By (23) and an elementary result in functional analysis,

$$\|\mathcal{J}_\Theta^\top \mathcal{J}_\Theta\| = \|\mathcal{J}_\Theta\|^2 \leq \left(\|I\| + \left\| \frac{dT_\Theta}{du} \right\| \right)^2 \leq (1 + \gamma)^2. \quad (29)$$

Hence

$$\|u\|^2 = \langle u, u \rangle = \langle \mathcal{J}_\Theta^{-1} u, (\mathcal{J}_\Theta^\top \mathcal{J}_\Theta) \mathcal{J}_\Theta^{-1} u \rangle \leq (1 + \gamma)^2 \|\mathcal{J}_\Theta^{-1} u\|^2, \quad \text{for all } u \in \mathcal{U}. \quad (30)$$

Combining (26) and (30) reveals

$$\frac{1 - \gamma}{(1 + \gamma)^2} \langle u, u \rangle \leq (1 - \gamma) \|\mathcal{J}_\Theta^{-1} u\|^2 \leq \langle \mathcal{J}_\Theta^{-1} u, \mathcal{J}_\Theta(\mathcal{J}_\Theta^{-1} u) \rangle = \langle \mathcal{J}_\Theta^{-1} u, u \rangle, \quad \text{for all } u \in \mathcal{U}. \quad (31)$$

This establishes (20), and we are done. \square

Lemma A.2. *If $A \in \mathbb{R}^{t \times t}$ is symmetric with positive eigenvalues,*

$$\bar{\lambda} \triangleq \frac{\lambda_{\max}(A) + \lambda_{\min}(A)}{2} \quad \text{and} \quad S \triangleq \bar{\lambda}I - A, \quad (32)$$

then

$$\|S\| = \frac{\lambda_{\max}(A) - \lambda_{\min}(A)}{2}. \quad (33)$$

Proof. Since A is symmetric, the spectral theorem asserts it possesses a set of eigenvectors that form an orthogonal basis for \mathbb{R}^t . This same basis forms the set of eigenvectors for $\bar{\lambda}I - A$, with eigenvalues denoted by $\{\lambda_i\}_{i=1}^t$. So, there exists orthogonal $P \in \mathbb{R}^{t \times t}$ and diagonal Λ with entries given by each of the eigenvalues λ_i such that

$$S = \bar{\lambda}I - P^\top \Lambda P = P^\top (\bar{\lambda}I - \Lambda) P. \quad (34)$$

Substituting this equivalence into the definition of the operator norm yields

$$\|S\| \triangleq \sup \{\|S\xi\| : \|\xi\| = 1\} = \sup \{\|P^\top (\bar{\lambda}I - \Lambda) P\xi\| : \|\xi\| = 1\}. \quad (35)$$

Leveraging the fact P is orthogonal enables the supremum above to be restated via

$$\|S\| = \sup \{\|(\bar{\lambda}I - \Lambda)P\xi\| : \|\xi\| = 1\} = \sup \{\|(\bar{\lambda}I - \Lambda)\zeta\| : \|\zeta\| = 1\}. \quad (36)$$

Because $\bar{\lambda}I - \Lambda$ is diagonal, (36) implies

$$\|S\| = \max_{i \in [t]} |\bar{\lambda} - \lambda_i| = \frac{\lambda_{\max}(A) - \lambda_{\min}(A)}{2}, \quad (37)$$

and the proof is complete. \square

Theorem 3.1. *If Assumptions 2.1, 3.1, 3.2, and 3.3 hold for given weights Θ and data d , then*

$$p_\Theta \triangleq - \left[\frac{\partial \ell}{\partial y} \left(\frac{dS_\Theta}{du} \frac{\partial T_\Theta}{\partial \Theta} + \frac{\partial S_\Theta}{\partial \Theta} \right) \right]_{(u,d)=(u_d^*,d)} \quad (38)$$

forms a descent direction for $\ell(y_d, \mathcal{M}_\Theta(d))$ with respect to Θ .

Proof. To complete the proof, it suffices to show

$$\left\langle \frac{d\ell}{d\Theta}, p_\Theta \right\rangle < 0, \quad \text{for all } \frac{d\ell}{d\Theta} \neq 0. \quad (39)$$

Let any weights Θ and data d be given, and assume the gradient $d\ell/d\Theta$ is nonzero. We proceed in the following manner. First we show p_Θ is equivalent to a preconditioned gradient (Step 1). We then show $M^\top d\ell/d\Theta$ is nonzero, with M as in (14) of Assumption 3.3 (Step 2). These two results are then combined to verify the descent inequality (39) for the provided Θ and d (Step 3).

Step 1. Denote the dimension of each component of the gradient $d\ell/d\Theta$ using¹⁰

$$\frac{\partial T_\Theta}{\partial \Theta} \in \mathbb{R}^{p \times n}, \quad \mathcal{J}_\Theta^{-1} \in \mathbb{R}^{n \times n}, \quad \frac{\partial S_\Theta}{\partial \Theta} \in \mathbb{R}^{p \times c}, \quad \frac{dS_\Theta}{du} \in \mathbb{R}^{n \times c}, \quad \frac{\partial \ell}{\partial y} \in \mathbb{R}^{c \times 1}. \quad (40)$$

Combining each of these terms yields the gradient expression¹¹

$$\frac{d\ell}{d\Theta} = \left[\frac{\partial T_\Theta}{\partial \Theta} \mathcal{J}_\Theta^{-1} \frac{dS_\Theta}{du} + \frac{\partial S_\Theta}{\partial \Theta} \right] \frac{\partial \ell}{\partial y}. \quad (41)$$

By Assumption 3.2, S_Θ and T_Θ depend on separate components of $\Theta = (\theta_S, \theta_T)$. Thus,

$$\frac{d\ell}{d\Theta} = \left[\begin{array}{c} \frac{\partial S_\Theta}{\partial \theta_S} \\ \frac{\partial T_\Theta}{\partial \theta_T} \mathcal{J}_\Theta^{-1} \frac{dS_\Theta}{du} \end{array} \right] \frac{\partial \ell}{\partial y} = \underbrace{\left[\begin{array}{cc} \frac{\partial S_\Theta}{\partial \theta_S} & 0 \\ 0 & \frac{\partial T_\Theta}{\partial \theta_T} \end{array} \right]}_M \underbrace{\left[\begin{array}{cc} \mathbf{I} & 0 \\ 0 & \mathcal{J}_\Theta^{-1} \end{array} \right]}_{\tilde{\mathcal{J}}_\Theta^{-1}} \underbrace{\left[\begin{array}{c} \mathbf{I} \\ \frac{dS_\Theta}{du} \end{array} \right]}_v \frac{\partial \ell}{\partial y}, \quad (42)$$

where we define¹² $M \in \mathbb{R}^{p \times (n+c)}$, $\tilde{\mathcal{J}}_\Theta^{-1} \in \mathbb{R}^{(n+c) \times (n+c)}$, and $v \in \mathbb{R}^{(n+c) \times 1}$ to be the underbraced quantities. This enables the gradient to be concisely expressed via the relation

$$\frac{d\ell}{d\Theta} = M \tilde{\mathcal{J}}_\Theta^{-1} v, \quad (43)$$

and our proposed gradient alternative in (38) is given by

$$p_\Theta = -Mv. \quad (44)$$

Because M has full column rank (by Assumption 3.3), $M^+ M = \mathbf{I}$, enabling us to rewrite p_Θ via

$$p_\Theta = -M \tilde{\mathcal{J}}_\Theta M^+ M \tilde{\mathcal{J}}_\Theta^{-1} v = -(M \tilde{\mathcal{J}}_\Theta M^+) \frac{d\ell}{d\Theta}. \quad (45)$$

Hence p_Θ is a preconditioned gradient (n.b. the preconditioner is not necessarily symmetric).

Step 2. Set

$$w \triangleq M^\top \frac{d\ell}{d\Theta} = M^\top M \tilde{\mathcal{J}}_\Theta^{-1} v. \quad (46)$$

The fact that M has full column rank implies it has a trivial kernel. In particular,

$$0 \neq \frac{d\ell}{d\Theta} = M \tilde{\mathcal{J}}_\Theta^{-1} v \implies 0 \neq \tilde{\mathcal{J}}_\Theta^{-1} v. \quad (47)$$

¹⁰We assumed each space is a real-valued finite dimensional Hilbert space, making it equivalent to some Euclidean space. So, it suffices to show everything in Euclidean spaces.

¹¹In the main text, the ordering was used to make clear application of the chain rule, but here we reorder terms to get consistent dimensions in each matrix operation.

¹²Note this choice of M coincides with the matrix M in Assumption 3.3.

Again leveraging the full column rank of M , we know $M^\top M$ is invertible and, thus, has trivial kernel as well. This fact together with (47) reveals

$$0 \neq (M^\top M) \tilde{\mathcal{J}}_\Theta^{-1} v = w. \quad (48)$$

Step 3. Inserting the definition of w and p_Θ formulation of (45) into the scalar product in (39) yields

$$\left\langle \frac{d\ell}{d\Theta}, p_\Theta \right\rangle = - \left\langle M^\top M \tilde{\mathcal{J}}_\Theta^{-1} v, \tilde{\mathcal{J}}_\Theta M^\top M \tilde{\mathcal{J}}_\Theta^{-1} v \right\rangle = - \left\langle w, \tilde{\mathcal{J}}_\Theta (M^\top M)^{-1} w \right\rangle, \quad (49)$$

noting $M^+ = (M^\top M)^{-1} M^\top$. Let λ_+ and λ_- be the maximum and minimum eigenvalues of $(M^\top M)^{-1}$, respectively. Note $(M^\top M)$ is positive definite since the full column rank of M implies

$$\langle \xi, M^\top M \xi \rangle = \|M \xi\|^2 > 0, \quad \text{for all nonzero } \xi \in \mathbb{R}^{n+c}. \quad (50)$$

Thus, $(M^\top M)^{-1}$ is positive definite, making $\lambda_+, \lambda_- > 0$. Let $\bar{\lambda}$ be the average of these terms, *i.e.*

$$\bar{\lambda} \triangleq \frac{\lambda_+ + \lambda_-}{2}. \quad (51)$$

Substituting in this choice of $\bar{\lambda}$ to (49) by adding and subtracting $\bar{\lambda} \mathbf{I}$ gives the inequality

$$- \left\langle w, \tilde{\mathcal{J}}_\Theta (M^\top M)^{-1} w \right\rangle \leq -\bar{\lambda}(1 - \gamma) \|w\|^2 + \left\langle w, \tilde{\mathcal{J}}_\Theta (\bar{\lambda} \mathbf{I} - (M^\top M)^{-1}) w \right\rangle, \quad (52)$$

noting $\tilde{\mathcal{J}}_\Theta$ is $1 - \gamma$ coercive because it is the block diagonal composition of \mathcal{J}_Θ , which is $1 - \gamma$ coercive by (19) in Lemma A.1, and the identity matrix, which is 1-coercive. Application of the Cauchy Schwarz inequality to the right hand side of (52) reveals

$$- \left\langle w, \tilde{\mathcal{J}}_\Theta (M^\top M)^{-1} w \right\rangle \leq -\bar{\lambda}(1 - \gamma) \|w\|^2 + \|\tilde{\mathcal{J}}_\Theta\| \|\bar{\lambda} \mathbf{I} - (M^\top M)^{-1}\| \|w\|^2. \quad (53)$$

By Lemma A.2,

$$\|\bar{\lambda} \mathbf{I} - (M^\top M)^{-1}\| = \frac{\lambda_+ - \lambda_-}{2}. \quad (54)$$

Similar block diagonal argument as used above to verify $\tilde{\mathcal{J}}_\Theta$ is coercive can also be applied to bound the operator norm of $\tilde{\mathcal{J}}_\Theta$. Indeed, (24) implies

$$\|\mathcal{J}_\Theta\| \leq 1 + \gamma \implies \|\tilde{\mathcal{J}}_\Theta\| \leq 1 + \gamma. \quad (55)$$

Hence (49), (53), (54), and (55) together yield

$$\left\langle \frac{d\ell}{d\Theta}, p_\Theta \right\rangle \leq -\frac{1}{2}((1 - \gamma)(\lambda_+ + \lambda_-) - (1 + \gamma)(\lambda_+ - \lambda_-)) \|w\|^2 = -2(\lambda_- - \gamma\lambda_+) \|w\|^2. \quad (56)$$

The right hand expression in (56) is negative since (48) shows $w \neq 0$ and the conditioning inequality (15) in Assumption 3.3 implies $(\lambda_- - \gamma\lambda_+)$ is positive. This verifies (39), completing the proof. \square

Corollary 3.1. *Given weights Θ and data d , there exists $\varepsilon > 0$ such that if $u^\varepsilon \in \mathcal{U}$ satisfies $\|u_d^\varepsilon - u_d^*\| \leq \varepsilon$ and the assumptions of Theorem 3.1 hold, then*

$$p_\Theta^\varepsilon \triangleq - \left[\frac{\partial \ell}{\partial y} \left(\frac{dS_\Theta}{du} \frac{\partial T_\Theta}{\partial \Theta} + \frac{\partial S_\Theta}{\partial \Theta} \right) \right]_{(u,d)=(u_d^\varepsilon,d)} \quad (57)$$

is a descent direction for the loss function $\ell(y_d, \mathcal{M}_\Theta(u_d^*, d))$ with respect to Θ .

Proof. For notational convenience, for all $\tilde{u} \in \mathcal{U}$, define

$$p_\Theta(\tilde{u}) \triangleq - \left[\frac{\partial \ell}{\partial y} \left(\frac{dS_\Theta}{du} \frac{\partial T_\Theta}{\partial \Theta} + \frac{\partial S_\Theta}{\partial \Theta} \right) \right]_{(u,d)=(\tilde{u},d)}, \quad (58)$$

noting $p_\Theta^\varepsilon = p_\Theta(u_d^\varepsilon)$. Also define the quantity

$$\nabla \triangleq \frac{d}{d\Theta} [\ell(y_d, \mathcal{M}_\Theta(d))]. \quad (59)$$

Assuming $\nabla \neq 0$, it suffices to show

$$\langle p_\Theta^\varepsilon, \nabla \rangle < 0. \quad (60)$$

By the smoothness of ℓ , S_Θ , and T_Θ (see Assumption 3.1), there exists $\delta > 0$ such that

$$\|u - u_d^*\| \leq \delta \implies \|p_\Theta(u) - p_\Theta(u_d^*)\| \leq \frac{(\lambda_- - \gamma\lambda_+) \|M^\top \nabla\|^2}{\|\nabla\|}, \quad (61)$$

where λ_+ and λ_- are the maximum and minimum eigenvalues of $(M^\top M)^{-1}$, respectively. Substituting the inequality (56) in the proof of Theorem 3.1 into (60) reveals

$$\langle p_\Theta(u), \nabla \rangle = \langle p_\Theta(u_d^*), \nabla \rangle + \langle p_\Theta(u) - p_\Theta(u_d^*), \nabla \rangle \quad (62a)$$

$$\leq -2(\lambda_- - \gamma\lambda_+) \|M^\top \nabla\|^2 + \langle p_\Theta(u) - p_\Theta(u_d^*), \nabla \rangle. \quad (62b)$$

But, the Cauchy Schwarz inequality and (61) enable us to obtain the upper bound

$$|\langle p_\Theta(u) - p_\Theta(u_d^*), \nabla \rangle| \leq (\lambda_- - \gamma\lambda_+) \|M^\top \nabla\|^2, \quad \text{for all } u \in B(u_d^*, \delta), \quad (63)$$

where $B(u_d^*, \delta)$ is the ball of radius δ centered about u_d^* . Combining (62) and (63) yields

$$\langle p_\Theta(u), \nabla \rangle \leq -(\lambda_- - \gamma\lambda_+) \|M^\top \nabla\|^2, \quad \text{for all } u \in B(u_d^*, \delta). \quad (64)$$

In particular, this shows (60) holds when we set $\varepsilon = \delta$. \square

B Classification Accuracy Plots

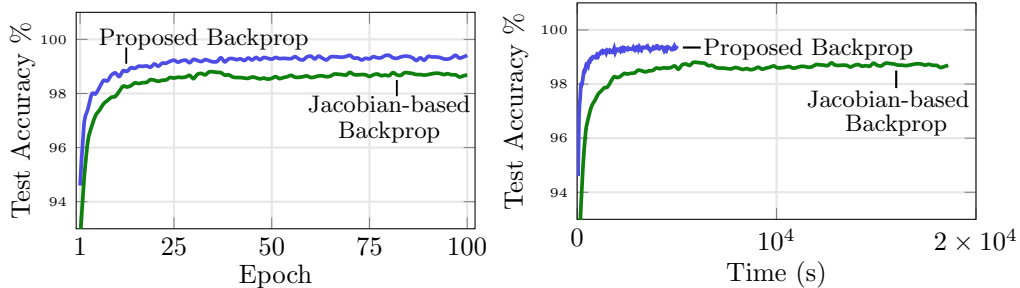


Figure 6: MNIST performance using identical models/configurations, but with two backpropagation schemes: our proposed method (blue) and the standard Jacobian-based backpropagation in (11) (green), with fixed point tolerance $\epsilon = 10^{-4}$. Our method is 4X faster and yields better test accuracy.

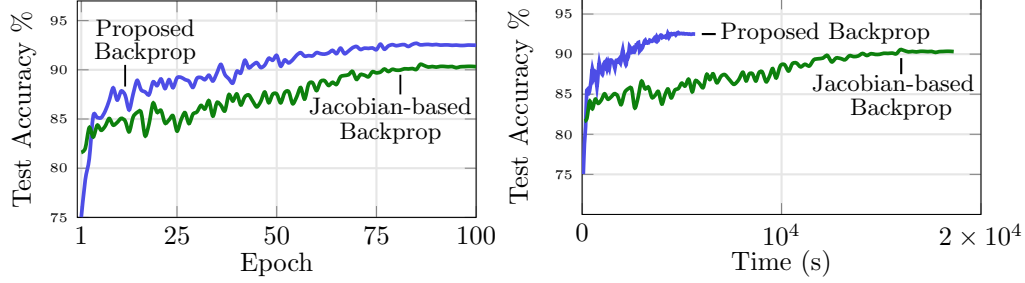


Figure 7: SVHN performance using identical models/configurations, but with two backpropagation schemes: our proposed method (blue) and the standard Jacobian-based backpropagation in (11) (green), with fixed point tolerance $\epsilon = 10^{-4}$. Our method is 3X faster and yields better test accuracy.

C Experimental Settings

We present the experimental settings and describe the architecture used for each dataset. For all models, we use the Adam [35] optimizer for training.

C.1 MNIST

We use two convolutions for the data-space portion of the network $Q(d)$ and use one fully-connected layer for the latent space with relu activation. For the fixed point stopping criterion, we stop whenever the fixed point satisfies $\epsilon < 10^{-6}$ or 100 iterations have occurred. We use an initial learning rate of 10^{-5} and decay the learning rate by multiplying it by 0.98 every 10 epochs. To map from the latent space to inference space, S_Θ , we use a fully connected layer with a relu activation function. For the loss function, we found mean squared error to be most effective.

C.2 SVHN

We use two convolutions for the data-space portion of the network $Q(d)$ and use one fully-connected layer for the latent space with leaky relu activation. For the fixed point stopping criterion, we stop whenever the fixed point satisfies $\epsilon < 10^{-4}$ or 100 iterations have occurred. We use an initial learning rate of 10^{-3} and decay the learning rate using cosine annealing [46]. To map from the latent space to inference space, S_Θ , we use a fully connected layer with a softmax activation function. We use cross entropy for the loss function.

C.3 CIFAR10

For the unaugmented CIFAR10 results, we use three convolutions for the data-space portion of the network $Q(d)$ and use two fully-connected layer for the latent space with leaky relu activation. For the augmented CIFAR10 results, we use ResNet56 [28, 30] for the data-space portion of the network $Q(d)$ and modify its final layer to output to a 45-dimensional latent space (rather than originally to 10 dimensional space). For the fixed point stopping criterion, we stop whenever the fixed point satisfies $\epsilon < 10^{-3}$ or 2000 iterations have occurred. We use an initial learning rate of 5×10^{-4} and decay the learning rate using cosine annealing [46]. To map from the latent space to inference space, S_Θ , we use a fully connected layer with a leaky relu activation function. We use cross entropy for the loss function.